ORIGINAL ARTICLE

Microstructure and Wear Behaviour of SS420 Micron Layers on Ti–6Al–4V Substrate Using Laser Cladding Process

N. Jeyaprakash[1,2] · Che-Hua Yang[1,2]

Abstract Ti–6Al–4V is commonly used material in automobile, aerospace, biomedical and marine due to its excellent properties. However, their uses are reduced because their its poor tribological performance. In the current study, stainless steel 420 alloy powder was cladded on Ti–6Al–4V base material using high-power Yb: YAG disc laser. Then, the cladded surfaces were evaluated to reveal their new phase formation, hardness changes and improved wear properties. Besides, the various wear mechanisms and their corresponding rough averages were studied. Results showed that the microhardness of laser cladded specimen is 613HV while base material shows 303HV. The wear rate of laser cladded specimen reduces remarkably compared to un-clad specimen. The identified major wear mechanisms are abrasive, adhesive and oxidation wear. The worn-out cladded surface shows lesser roughness than base material.

Keywords Ti–6Al–4V · SS420 · Laser cladding · Microstructure · Wear mechanism · Roughness

✉ N. Jeyaprakash
prakash84gct@gmail.com; prakash@ntut.edu.tw

Che-Hua Yang
chyang@ntut.edu.tw

1   Centre of Mass Customization Additive Manufacture, National Taipei University of Technology, Taipei, Taiwan, ROC

2   Institute of Manufacturing Technology, National Taipei University of Technology, Taipei, Taiwan, ROC

1 Introduction

Ti–6Al–4V is commonly used material in automobile, aerospace, biomedical and marine because of good properties such as low cost, higher strength and good corrosion properties. However, their uses are reduced because of its poor tribological performance [1]. So, there is a necessary to enhance the surface properties of titanium alloys for its wider usage. In recent years, there are many techniques such as laser surface-level treatment, plasma transfer arc welding (PTAW), electro-plating and thermal spraying. Among those surfacing methods, laser material processing is followed in many applications due to its higher cooling rates [2]. Laser-based surface treatment can be divided into several methods such as hardening, alloying, texturing and cladding [3]. From the above-mentioned methods, laser cladding is recognized as a promising technique due to their higher bonding strength between base material and coating. This laser processing can melt the base material surface with reduced heat-affected zone (HAZ) [4]. In addition, the alloy powders are sprayed towards the base material with good quality and less dilution which can properly bond on the surface of material. So, the engineers and investigators have focussed to study the laser cladding process to attain an enhanced surface property.

The pre-mixed tough alloy powders have been identified as a main solution to improve the wear properties of the metallic plates. In recent years, cobalt-, nickel- and steel-based nanoparticle are identified and used as coating material to protect the surfaces from sliding wear. Among those nanoparticles, steel-based powders are more attractive due to its less cost, higher hardness and good wear properties. García-Rodríguez et al. [5] studied the corrosion properties of magnesium alloy using high-velocity oxy-fuel (HVOF)-coated steel particles. The outcomes

indicated that the corrosion behaviour was enhanced on steel coating surface while compared with magnesium surface. Lou et al. [6] investigated the friction and wear behaviour of steel coating on Al–Si surface using plasma-transferred wire arc (PTWA) method. The outcomes represent that the wear resistance was improved on the coating surface. Baiamonte et al. [7] studied the wear properties of cobalt-coated steel material using plasma-transferred arc (PTA) method. The results showed that the mechanical and tribological properties were improved. Mathieu Marquer et al. [8] studied the wear behaviour of CoCrAlYSiBN-coated titanium alloy using atmospheric plasma spray (APS) method and concluded that the wear rate was reduced on the coated specimen while compared with uncoated specimen.

Mao and his co-worker [9] conducted sliding wear study with different applied loads on titanium alloy and concluded that the material loss was increased slightly while increasing the applied load. Jun and co-worker [10] examined the wear behaviour of titanium alloy with various sliding speed and concluded that the formation of oxides reduced the wear rate. Li et al. [11] investigated the wear properties and various mechanisms on T-64 alloy by different sliding velocities. The obtained results indicated that oxidation and delamination were a major wear mechanisms at lower and higher sliding speed, respectively. From the above literature, the techniques such as HVOF, PTWA and APS were used to improve the surface properties. However, no investigation has been found on the wear behaviour of steel-coated titanium alloy using laser cladding process. The laser-based surface treatment becomes more wide in the present mechanical industries, and the direction of investigation has changed from traditional to modern techniques, i.e. from hardening to laser cladding processes [12]. In the current study, stainless steel (SS) 420 alloy powder was cladded on Ti–6Al–4V base material using high-power Yb: YAG disc laser. Then, the cladded surfaces were evaluated to reveal their new phase formation, hardness changes and improved wear properties. Besides, the various wear mechanisms and their corresponding rough averages were studied.

2 Experimental Procedure

Commercially available Ti–6Al–4V plate with the dimensions of 3.5 cm × 3.5 cm × 0.5 mm was used as base material. The base material surface was cleaned with acetone and sand blasted to obtain a roughness of ~ 6 microns for better bond strength between coating and base material. The alloy powder SS 420 was used as coating material with the particle size of 25–130 microns. The elemental composition of alloy powder and base material is given in Table 1. The cladding parameters such as particle flow rate, power and scanning speed were varied and optimal parameters were found to coat the alloy powder on Ti–6Al–4V plate using 4 kW Yb: YAG disc. The identified optimal laser cladding parameters is given in Table 2. Further, the laser-coated specimens were cross-sectioned using wire electrical discharge machine (WEDM) to study their new phase formation, hardness and microstructure. Besides, ball on plate tribometer was used to study the wear resistance of coating and compared with base material. The hardened WC ball was used as counterpart with the diameter of 6.22 mm. The followed wear study parameters were load (35 N), sliding distance (1500 M) and sliding velocity (0.5 m/s). The loss of material was measured for cladded and un-cladded specimens and compared. The various wear mechanisms and roughnesses of worn-out specimen were studied using scanning electron microscopy (SEM) and whitelight interferometer, respectively. Figure 1 represents the SEM images of alloy powder (a), schematic of laser processing (b) and clad cross section with geometrical characteristics (c).

Table 2 Laser cladding parameters

Power	1000 W
Scanning speed	600 mm/min
Feed rate	7 g/min
Spot size	3.2 mm
Stand-off	15 mm
Preheating	150 °C
Overlapping	50%
Powder carrier gas (argon)	6 SD@1 bar
Shielding gas (argon)	25 lpm

Table 1 Chemical composition of substrate and powder

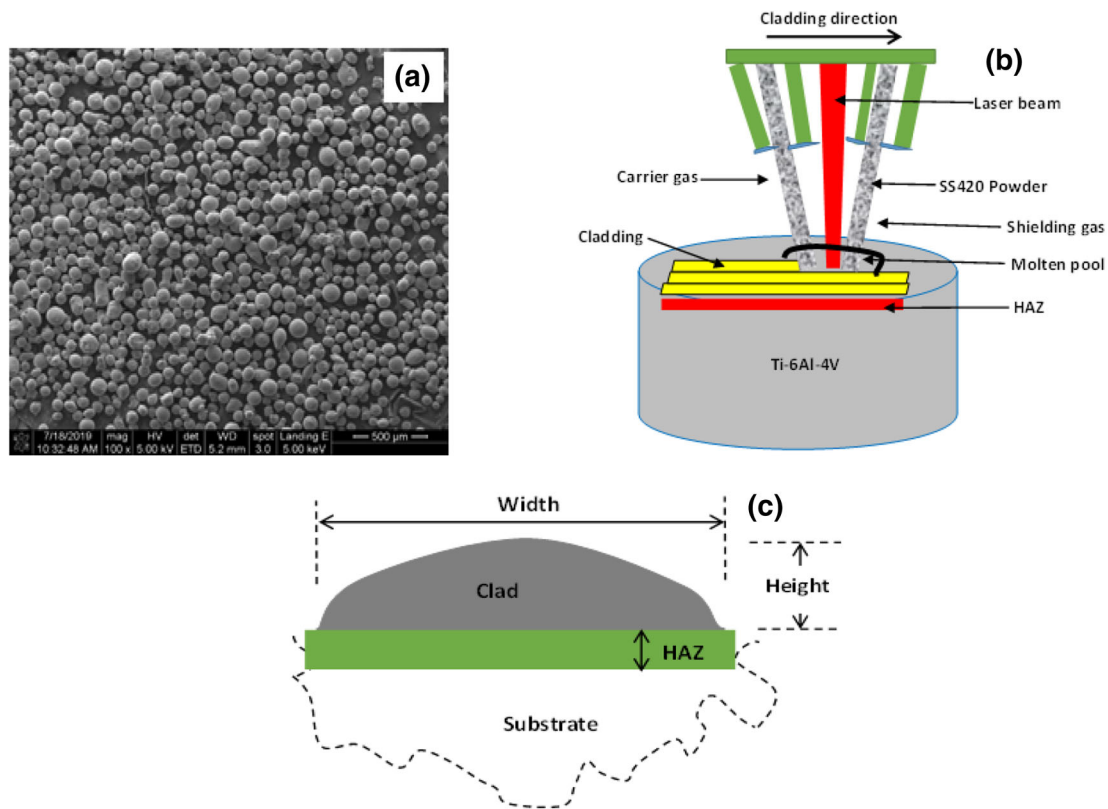| Materials	Elements composition (wt%)								
	Ti	Cr	Fe	Al	C	Si	Mo	Mn	V
Substrate (Ti–6Al–4V)	Bal	0.008	0.121	5.87	0.342	–	0.006	–	3.89
SS 420 Powder	–	14.1	Bal	–	0.17	1.02	–	0.97	–

Fig. 1 SEM images of SS420 powder (**a**), schematic picture of laser cladding system (**b**) and clad cross section with geometrical characteristics (**c**)

3 Results and Discussion

3.1 Structural Analysis

Figure 2a shows the SEM image of SS420 deposition with various three regions, namely cladding, heat-affected zone (HAZ) and substrate. The cladding regions show martensite dendrites across the cladding deposition. The temperature during laser cladding process causes three various structures like cellular dendrite, equiaxed dendrites and lengthy needle like structure is formed on HAZ [13]. Practically, consistent structure has been identified across the cladding region, even at centre of the deposition region and overlapping regions. Besides, the coating region exhibits no defects such as crack and pits. A proper bonding is observed between base material and coating material because the identified laser parameters are optimal and produce no defects. In addition, it is important to analyse the coating–substrate interface to prove its bonding strength. Some times, the deposited layer can be peeled off with reduced adhesion properties and chances for delamination is higher because of thermal mismatch. Besides, there is a possibility for cracks due to brittle nature of intermetallic elements. The measured coating thickness is 627.655 ± 08 μm. The HAZ reduces due to optimal laser

cladding parameters, and the coating thickness is also lesser. If the thickness is more, there may be possibility for brittle nature on the interface region. Therefore, there is no possibility of crack on the interface region of coating. Figure 2b shows the magnified view of HAZ. Further, the cladding region shows Fe in martensite phase on the cladded surface which can protect the surface from the externally applied load [14]. The corresponding elemental analysis shows Fe (63.7%) as a major element along with Mn (1.7%) and Cr (22.7%) elements. Figure 2c represents the cladding zone with elemental analysis (d).

3.2 Microhardness and Phase Analysis

Figure 3a shows the hardness profile of laser cladded specimen. The hardness profile indicates that there are three different regions, namely cladded region, HAZ and substrate. The cladded region improves the hardness and the average values are ~ 613HV while applied with 300 g load and 15 s dwell time. The observed hardness on the HAZ is 476.5HV due to coarse structure. The microhardness is a significant property which can affect the wear properties of the material. The noticed hardness on the cladding surface is two times higher than base material. The achieved higher hardness on the cladding region is due
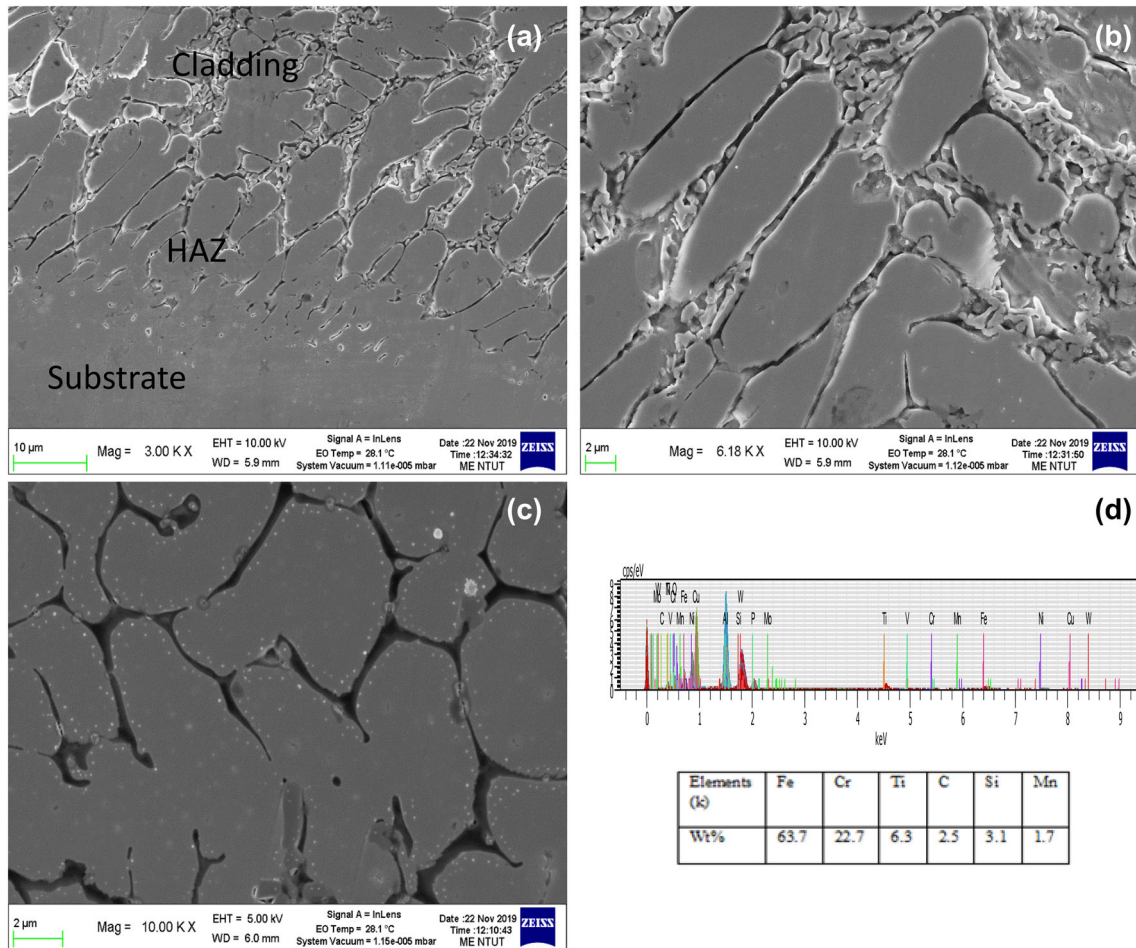
Fig. 2 SEM images showing three various regions, namely cladding, HAZ and substrate (**a**), magnified view of HAZ (**b**), magnified picture of cladding region (**c**) and elemental analysis indicating the presence of iron content (**d**)
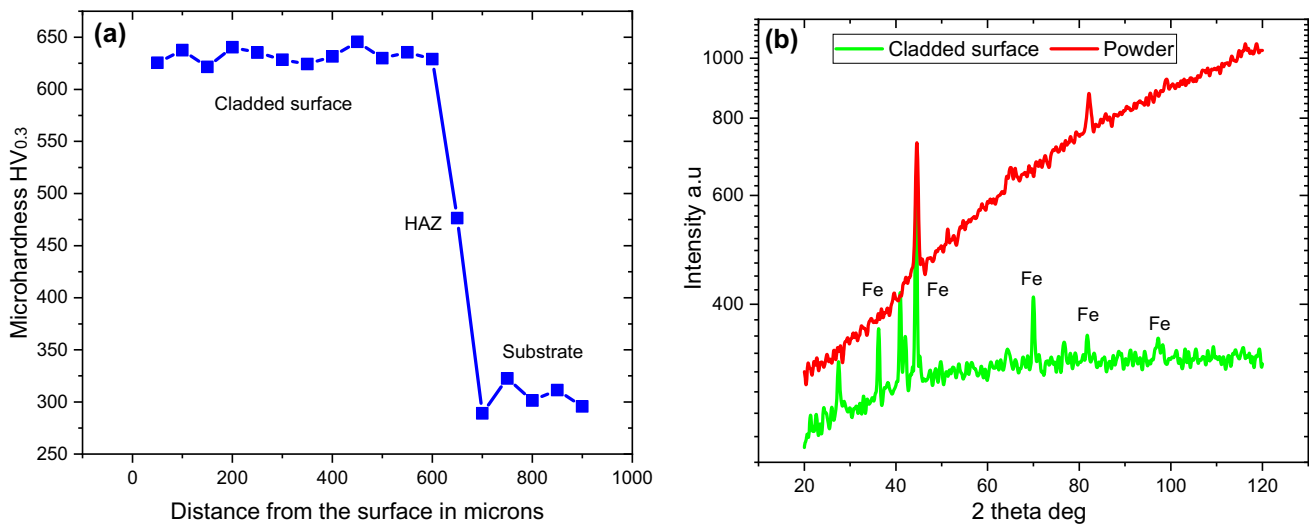

Fig. 3 Microhardness profile (**a**), phase analysis (**b**)

to combined results such as hard phases, defect free and optimal cladding parameters [15]. The greater microhardness in the deposited layer indicates that it will work better as a surface protecting material under higher applied loads. Practically, greater the microhardness, the lower the wear rate [16]. The achieved higher hardness on the deposited layer is due to formation of martensite as proved from the structural analysis. From the phase analysis, it is clear that the Fe peaks are major after laser cladding process. No reaction happens during cladding period. So, there is no changes in the martensite phase after deposited SS420 particle on Ti–6Al–4V surface. Figure 3b shows the phase analyses of powder and laser cladded surface.

3.3 Wear and Friction Study

Sliding wear study process normally includes several factors such as applied load, temperature and physical properties [17]. The wear rate of un-clad titanium alloy shows linear increase while increasing the sliding distance. It is clearly identified that un-clad specimen shows various wear regularities under the selected conditions. It shows poor wear resistance when compared to cladded specimen. When increasing the sliding distance from 300 to 1000 m, the wear rate also increases to 0.085 mm^3/m. This larger differences of wear rate as a function of sliding distance seems to be a major scientific significance. Figure 4a shows the wear graph of un-clad and clad surfaces.

Figure 4b indicates the friction coefficient (CoF) of base material and laser cladded specimen. It can be noticed that CoF varies in base material as the sliding distance increases. In the beginning, the CoF is less when it reaches 100 m distance. However, while increasing the sliding distance to 1500 m, the CoF reaches the maximum level of 0.67. At the same time, the laser cladded specimen indicates the lesser CoF while compared with base material. The maximum CoF reaches to 0.45 while the sliding distance is 1500 m. The CoF is directly related to wear resistance of material. The lower CoF exhibits higher wear resistance and higher CoF produces more wear rate. In the present study, it correlates well while comparing the CoF and wear rate of clad and un-clad specimens. Further, the deposited alloy powders enhances the hardness of base material after laser processing. The formed structure with the combination of iron and chromium enhances the wear resistance. Besides, it increases the load carrying capacity and reduces the mechanical damages from the possible wear scratches.

3.4 Wear Mechanism and Roughness Analysis

Figure 5a shows the worn-out surface of base material. The worn surface shows various wear morphologies like debris and pulling out the metal. Severe wear can be noticed on the base material surface. There are many severe grooves, and delaminated particle can be observed on the base material surface. The lesser hardness of substrate is heavily influenced during the wear study. Besides, laser cladded specimen shows minimum wear loss when related to base material. The improved hardness influences more on the cladded surface during wear experiment. The observed microparticles are very less on the cladded worn-out surface. Figure 5c shows the worn-out SEM images of cladded surface. The direct contact between ball and disc produces the micro-abrasive particle on the worn-out surface during sliding. Those micro-abrasive particles permanently stay on the contact surface and further promote the excess material loss [18]. During this period, the counterpart can form severe wear track on the specimen
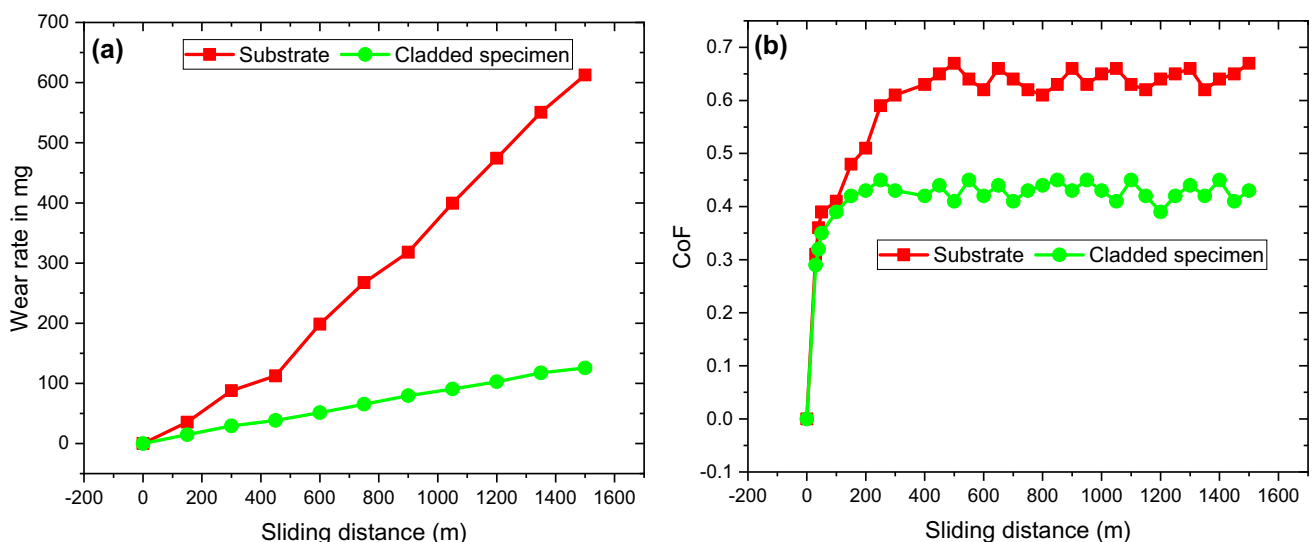

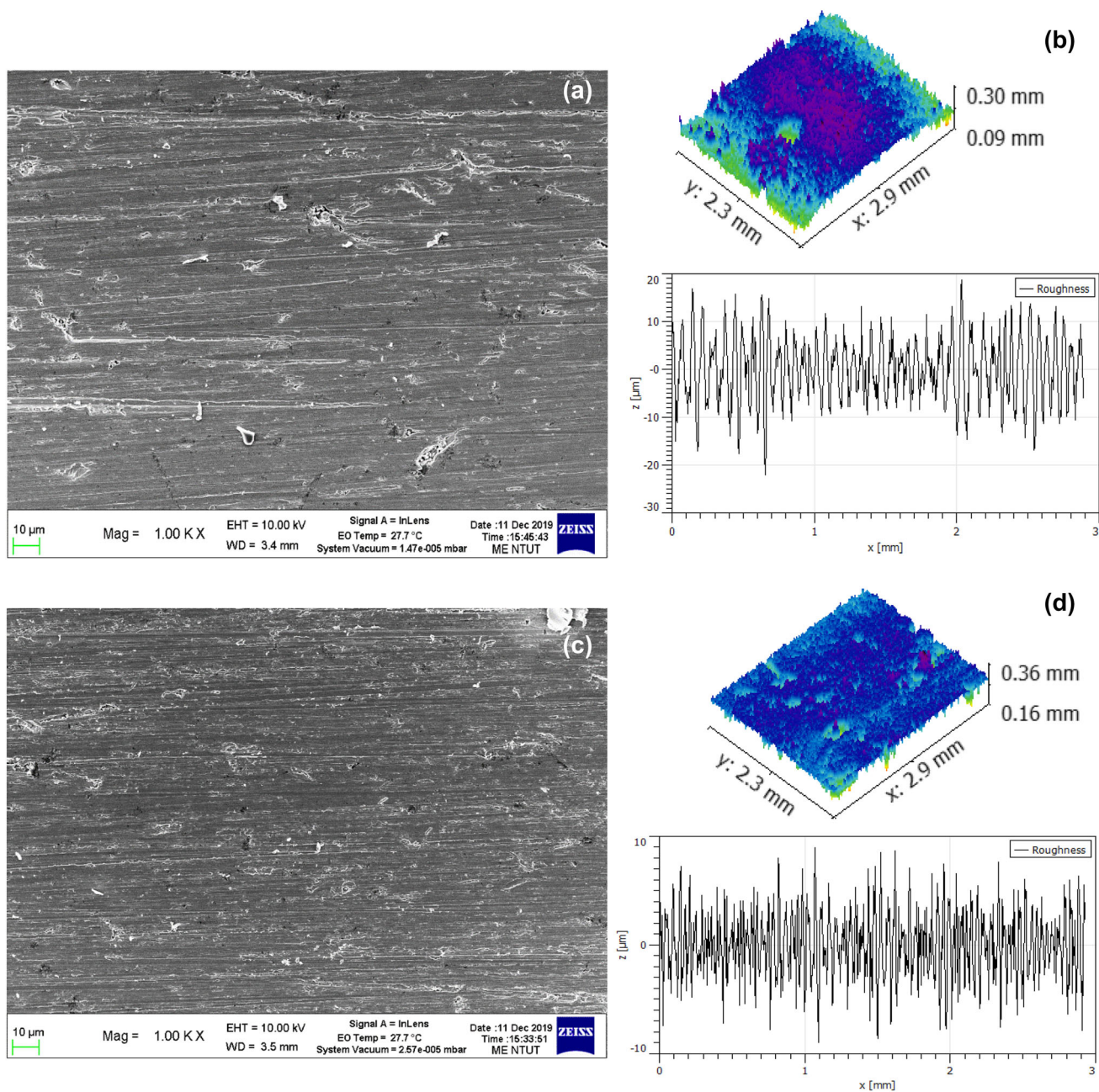Fig. 4 Mass loss (a), coefficient of friction (b) for substrate and laser cladding samples

Fig. 5 SEM picture of worn-out surface **a** substrate, **c** laser cladded specimen and their corresponding roughness average (**b** and **d**)

surface. In addition, the harder ball can plough out the softer material from the specimen. As an outcome, adhesion and scuff may have occurred. Further, continuous sliding can increase the heat between the sliding contact surfaces. Based on this heat source, the tribo-oxide layers are formed on the sliding surface and they protect the cladded specimen from the material loss. Also, the wear behaviour of titanium alloys also can form the protective oxide layer during continuous sliding at higher temperature [9, 19–21]. The reduced material loss and nonappearance of adhesive and delamination on the cladded worn-out

surface due to improved microhardness provides the hard alloy powders. Also, the wear resistance and hardness of the material are correlated with each other well as per the Archard's wear law [22]. During abrasion wear stage, one part of energy is consumed from the total energy to cut, plough and deform the material. Here, the deformed particle will promote the work hardening process on the sliding surface and reduce the wear rate possibly. Still, after sliding some few hundred metre distance, the wear rate becomes stable and removes the material constantly [23]. The minimized wear rate on the cladded surface is not

only based on the improved hardness. The improved wear properties are based on the alloy powders, particle distribution during cladding process and powder grain size [24]. Besides, the particle iron and chromium are evenly distributed on the cladding surface and the counterpart contacts of the sliding surface and produces oxide layer on the clad surface [25]. This produced oxide layer successfully protects the surfaces from the damages. The roughness average of base material worn surface is higher (5.6 micron) due to its minimum hardness and wear resistance. However, the roughness average of cladded surface is shown with lesser value (2.6 microns) because of its improved hardness and wear resistance. Figure 5b, d shows the roughness average of worn-out surface of substrate and laser cladded specimen, respectively.

4 Conclusion

Phase analysis, hardness and wear characteristic of SS 420 laser cladded specimen were studied and compared with base material. Based on the obtained results, the following conclusions were drawn.

- Coating region exhibits no defects such as crack and pits. Proper bonding is observed between base material and coating material. Further, cladding regions show martensite dendrites across the deposition.
- The cladding region shows Fe in martensite phase on the surface which can protect the surface from the externally applied load
- The achieved higher hardness on the cladding region is due to combined results such as hard phases, defect free and optimal cladding parameters. From the phase analysis, Fe peaks are major after laser cladding process.
- The wear rate of un-clad titanium alloy shows linear increase while increasing the sliding distance.
- Abrasive, adhesion and delamination are the major wear mechanisms for the substrate while laser cladded specimen shows mild abrasive and oxide layers. The laser cladded specimen reduces the roughness average due to lesser wear rate.

References

1. Kuriachen B, Lijesh K P, and Kuppan P, *Trans Indian Inst Met* **71** (2018) 1331.
2. Jeyaprakash N, Yang C-H, and Tseng S-P, *Int J Adv Manuf Technol* **106** (2019) 2347.
3. Jeyaprakash N, Yang C-H, and Sivasankaran S, *Mater Manuf Process* **35** (2019) 142.
4. Liu F, Ji Y, Sun Z, Wang G, and Bai Y, *Mater Manuf Process* **34** (2019) 1458.
5. García-Rodríguez S, Torres B, Pulido-González N, and Otero E, *Surf Coat Technol* **378** (2019) 124994.
6. Lou M, Whiteb D R, Banerjia A, Alpas A T, *Wear* **432** (2019) 102921.
7. Baiamonte L, Tuluic M, Bartuli C, Marini D, Marino A, Menchetti F, Pileggic R, Pulci G, and Marra F, *Surf Coat Technol* **371** (2019) 322.
8. Marquer M, Philippon S, Faure L, Chassaing G, Tardelli J, and Demmou K, *Tribol Int* **136** (2019) 13.
9. Mao Y S, Wang L, Chen K M, Wang S Q, and Cui X H, *Wear* **297** (2013) 1032.
10. Qu J, Blau P J, Watkins T R, Cavin O B and Kulkarni N S, *Wear* **258** (2005) 1348.
11. Li X X, Zhou Y, Ji X L, Li Y and Wang S Q, *Tribol Int* **91** (2015) 228.
12. Arayibi P K, Abioye T E, Clare A T, *Int J Adv Manuf Technol* **87** (2016) 3349.
13. Roy T, Lai Q, Abrahams R, Mutton P, Paradowska A, Soodi M, and Yan W, *Wear* **412–413** (2018) 69.
14. Gao F, Liu R, Wu X J, *Thin Solid Films* **519** (2011) 4809.
15. Jeyaprakash N, Duraiselvam M, and Raju R, *Arch Metall Mater* **63** (2018) 1303.
16. Moore M, *Wear* 28 (1974) 59.
17. Jeyaprakash N, Yang C-H, Tseng S-P, *Metals Mater Int* (2019) https://doi.org/10.1007/s12540-019-00526-6.
18. Birol Y, *Wear* **269** (2010) 664.
19. Cui X H, Mao Y S, Wei M X, and Wang S Q. *Tribol Trans* **55** (2012) 185.
20. Wang L, Zhang Q Y, Li X X, Cui X H, Wang S Q, *Tribol Lett* **53** (2014) 511.
21. Wang L, Zhang Q Y, Li X X, Cui X H, and Wang S Q, *Metall Mater Trans* A **45** (2014) 2284.
22. Ramkumar K R, Sivasankaran S, Al-Mufadi F A, Siddharth S, and Raghu R, *Achieves Civ Mech Eng* **19** (2019) 428.
23. Jeyaprakash N, Duraiselvam M, and Aditya S V, *Surf Rev Lett* **26** (2019) 1950009.
24. Davis J R, ASM International, Metals Park, **6** (1993) 789.
25. Umanskii A P, Storozhenko M S, Hussainova I V, Terentiev A E, Kovalchenko A M and Antonov M M, *Powder Metall Metal Ceram* **53** (2015) 663.